Variability and Changes in Pearl River Delta Water Level: Oceanic and Atmospheric Forcing Perspectives

Xiangbo Feng,[a,b] Wei Zhang,[a] Zhenglei Zhu,[a] Amulya Chevuturi,[b,c] and Wenlong Chen[d]

[a] *State Key Laboratory of Hydrology-Water Resources and Hydraulic Engineering, Hohai University, Nanjing, China*
[b] *National Centre for Atmospheric Science and Department of Meteorology, University of Reading, Reading, United Kingdom*
[c] *UK Centre for Ecology & Hydrology, Wallingford, United Kingdom*
[d] *Pearl River Hydraulic Research Institute, Pearl River Water Resources Commission, Guangzhou, China*

ABSTRACT: Understanding water level (WL) fluctuations in river deltas is important for managing water resources and minimizing the impacts of floods and droughts. Here, we demonstrate the competing effects of atmospheric and oceanic forcing on multi-time-scale variability and changes in the Pearl River Delta (PRD) WLs in southern China, using 52 years (1961–2012) of in situ observations at 13 hydrological stations. PRD WL presents significant seasonal to decadal variations, with large amplitudes upstream related to strong variability of southern China rainfall, and with relatively small amplitudes at the coastal stations determined by sea level (SL) fluctuations of the northern South China Sea. We find that the strengths of atmospheric and oceanic forcing in PRD are not mutually independent, leading to a distinct contrast of WL–forcing relationships at upstream and coastal stations. In the transition zone, because of the counteraction of atmospheric and oceanic forcing, no robust relationships are identified between WL and either of the forcing. We further show that in the drought season of the warm ENSO and PDO epochs, the effect of atmospheric (oceanic) forcing on PRD WL is largely enhanced (weakened), due to increased southern China rainfall and negative SL anomalies. Over the observation period, WL significantly decreased at upstream stations, by up to 28–42 mm yr^{-1} for flood season, contrasting with the upward trends of <4.3 mm yr^{-1} at coastal stations across all seasons. Southern China rainfall explains little of the observed WL trends, while SL rise is mostly responsible for the WL trends at coastal stations.

KEYWORDS: Rivers; Climate variability; Hydrologic cycle; Hydrometeorology; Interannual variability; Interdecadal variability; Seasonal cycle; Trends

1. Introduction

Understanding changes and variability in water levels (WLs) of the river delta on various time scales is vital, e.g., for managing water resources and minimizing flood impacts. There are multiple natural factors influencing the river delta WL, including river discharge and sea level, alongside anthropogenic activities such as local water extraction and riverbed dredging. The Pearl River Delta (PRD) is a coastal region of southern China, adjacent to the South China Sea (SCS). In this region, the Pearl River has three major tributaries, namely, the West, North, and East Rivers, which are connected with minor distributaries (Fig. 1a), forming one of the most complicated river networks in the world (e.g., Zhang et al. 2009). Water security and flood risk, related to the compound effects of hydrometeorological extremes and intensive human activity, pose a major threat to economic development and social welfare in this region. In this paper, we evaluate the effects of

atmospheric and oceanic forcing on the PRD WL on time scales from seasonal to decadal. The evaluation methods used in this study can be applied to WL fluctuation analysis in other major river deltas and estuaries.

The PRD WL has changed significantly over the past decades. Many studies attributed the long-term trends of PRD WL to morphological changes in river channels (e.g., Luo et al. 2007; Zhang et al. 2008, 2011; Zhang et al. 2015; Z. Wu et al. 2016). Morphological evolution of PRD river channels is mainly caused by human activities. The large-scale river-dredging and sand-mining activities deepened and widened the riverbed. The 1990s saw the most intensive excavation in the PRD, causing the mean WL to decrease dramatically; in the 1960s and 1970s prior to the China economic reform, the PRD WL decreased relatively slower due to lesser river-dredging and sand-mining activities. Further, inhomogeneous changes in river morphology significantly altered the streamflow ratio between the West River and North River (Luo et al. 2007), causing more water to flow to the North River distributaries and less to the West River distributaries. The streamflow redistribution could be partially responsible for the inhomogeneity of WL trends across the PRD (Chen et al. 2007; Zhang et al. 2009). So far, most studies focused on the effects of riverbed morphological changes on the annual-mean average of PRD WL. River WL substantially varies with seasons, but fewer studies addressed the seasonal variations of PRD WL trend. Furthermore, it remains largely unknown what roles the main natural forcing factors play in the changes of PRD WLs.
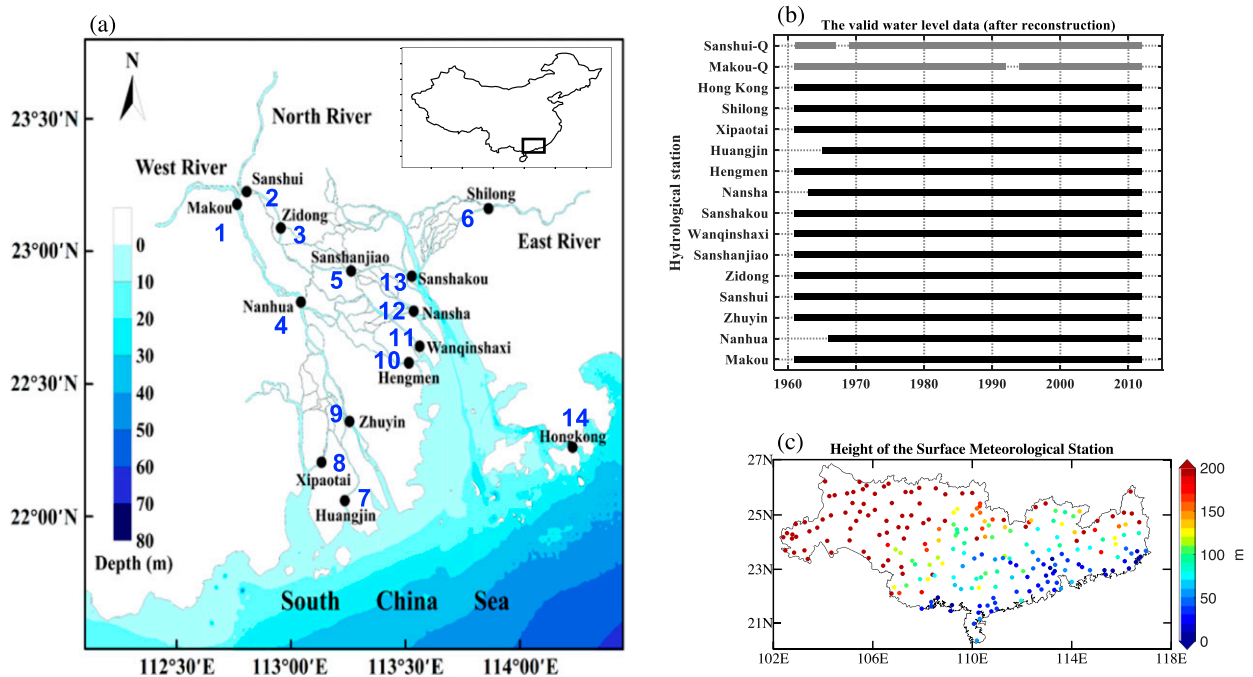
FIG. 1. (a) Map of the Pearl River Delta (PRD) and locations of 13 hydrological stations, including tide gauge station at Hong Kong. The stations are numbered coastward from 1 to 14: 1) Makou, 2) Sanshui, 3) Zidong, 4) Nanhua, 5) Sanshanjiao, 6) Shilong, 7) Huangjin, 8) Xipaotai, 9) Zhuyin, 10) Hengmen, 11) Wanqinshaxi, 12) Nansha, 13) Sanshakou, and 14) Hong Kong. (b) Quality-controlled hydrological and sea level data during 1961–2012. (c) The 222 rain gauge stations in the Pearl River catchment. In (c), color shows the heights of rain gauge stations above mean sea level.

The Pearl River streamflow is predominately associated with the rainfall in the river basin. Observations suggest no conclusive trend in the annual-mean precipitation in the Pearl River catchment over the past decades (Q. Zhang et al. 2012; Zhao et al. 2017; Deng et al. 2018). In contrast, summer rainfall and rainfall extremes significantly increased in southern China, resembling the prevailing ''north dry–south wet'' pattern of rainfall over eastern China (Chang et al. 2012; Duan et al. 2013; Ye et al. 2013). This dipole pattern of summer rainfall change could be associated with the weakening of the East Asia summer monsoon, which makes the rainband sluggish to move northward (e.g., Zhao et al. 2010). Interannual to interdecadal variations of PRD river streamflow could be associated with the rainfall anomalies modulated by the large-scale atmospheric and oceanic climate variability. However, Ouyang et al. (2014) found that the teleconnections from either El Niño–Southern Oscillation (ENSO) or the Pacific decadal oscillation (PDO) to the annual-mean streamflow of the Pearl River are weak and statistically unidentifiable. The lack of teleconnections to annual-mean streamflow might be due to the inconsistent relationships across seasons, which need further investigation. Variations and changes in PRD WL may not resemble these observed changes in river discharge and rainfall, as WL is determined by multiple factors, such as the shape of riverbed and river channel slope. Evaluating the response of PRD WL to regional precipitation, conditional on seasons and climate variability, is important for

understanding and attributing the long-term variability and changes in PRD WL.

Sea level (SL) is another important natural factor affecting PRD WL, by acting as the lower boundary conditions of the river networks. Seawater intrudes into the river channel from estuaries, which can ultimately alter the WLs. When SL is higher and/or river streamflow is lower, seawater can intrude further up. Mean SL in the northern part of SCS has risen by >2 mm yr^{-1} over the past 60 years, with accelerated rate in the most recent decades (e.g., Feng and Tsimplis 2014; Cheng et al. 2016; Feng and Cheng 2019). In the meantime, SL presents distinct temporal variability. Seasonal variations of SL at the SCS coasts can be more than 15 cm, related to surface wind stress and ocean thermal expansion (e.g., Feng et al. 2015; Cheng et al. 2016). On interannual and decadal time scales, ENSO and PDO are the main climate modes which can affect the SCS SLs (e.g., Cheng et al. 2016; Feng and Cheng 2019; Storto et al. 2019). However, as far as we know, no studies have rigorously assessed the effect of regional SLs on the changes and variability of PRD WL.

In this paper, we will investigate the causal influence of the atmospheric and oceanic forcings on the PRD WL, using more than 50 years of in situ observations. The atmospheric and oceanic forcings are approximated by the precipitation in the Pearl River catchment and SLs on the northern SCS, respectively. We address two key questions in this study: (i) how do local rainfall and SL affect the variability and changes in PRD WL, and (ii) how are these influences modulated by the

large-scale modes of climate variability? Attributing the individual and compound effects of natural forcing sources on PRD WL on various time scales will help us understand the main drivers for PRD WL variability and changes. This will also be beneficial in the future for such as developing empirical approaches to predict PRD WL.

The rest of the paper is organized as follows. In section 2, observations for WL, SL, and precipitation are described, along with the methodology. In sections 3a and 3b, the variability of PRD WL on time scales from seasonal to decadal is evaluated and interpreted by regional precipitation and SL. In section 3c, the teleconnections from ENSO and PDO to WL across different seasons are identified. Finally, in section 3d, the long-term trend in WL is analyzed and discussed. Conclusions and discussions are provided in section 4.

2. Data and methodology

We analyze daily WL records at 13 hydrological stations in the PRD (Fig. 1a) over the period of 1961–2012. WL records were digitalized from the hydrological yearbooks of China, with daily means produced by averaging two high and two low WLs in a lunar day (Zhang et al. 2009; Cao et al. 2020). These daily records are then averaged to monthly means only in months when at least 18 daily values (~60%) are valid. We also visually check the time series of monthly means at each station and removed spurious spiky values. Annual means of WL are calculated in those years when at least 9 monthly values are valid. Additionally, daily averaged river discharge was recorded at Makou and Sanshui stations during the same time period; we applied the same data-processing procedures as in WL. The river discharge data were also collected from the hydrological yearbooks of China (Zhang et al. 2009). Locations of these 13 hydrological stations in the PRD and the period of valid records at each station are shown in Figs. 1a and 1b.

In situ observations of precipitation and SL during 1961–2012 are also analyzed in our study. Daily accumulated precipitation data are obtained from China Meteorological Data Service Centre (National Meteorological Information Centre) of China Meteorological Administration (http://data.cma.cn/data/cdcindex/cid/00f8a0e6c590ac15.html). Our analysis only includes rain gauge observations in the Pearl River catchment (222 stations; Fig. 1c). SL at Hong Kong is approximated as the lower boundary for the PRD WL. Tide gauge records of monthly mean SL at Hong Kong are obtained from the Permanent Service for Mean Sea Level (https://www.psmsl.org). At Hong Kong, SL records at the North Point and Quarry Bay stations are combined to one continuous record after adjusting the datum to the same level, as in Feng and Tsimplis (2014).

The ENSO and PDO phenomena are taken as the large-scale modes of climate variability that could affect PRD WL. The indices of ENSO and PDO are obtained from the National Oceanic and Atmospheric Administration (NOAA) (https://psl.noaa.gov/data/climateindices/list) and the Joint Institute for the study of the Atmosphere and Ocean (JISAO) (http://jisao.washington.edu/pdo/PDO.latest), respectively. Here, the ENSO index is defined by the SST anomalies in the Niño-3.4 region (5°N–5°S, 170°–120°W) averaged over the boreal winter season of December–February (DJF), while the PDO index is defined as the leading principal component of North Pacific monthly sea surface temperature variability (monthly sea surface temperature anomalies in the North Pacific Ocean, poleward of 20°N) averaged over the 12 calendar months. The ENSO index is further filtered with a 7-yr high-pass filter, to retain the interannual variability, and the PDO index is filtered with an 11-yr low-pass filter, to retain the decadal variability.

3. Results

a. Seasonality of water level

1) VARIATIONS

Seasonal cycle of PRD WL is evaluated by averaging monthly WL anomalies over 1961–2012. In each year, annual mean was removed to eliminate the effects of long-term variability and trend, acting as a high-pass filter. WL in the PRD exhibits significant seasonal variations with a monomodal peak during the summer months and trough during the winter months (Fig. 2). Averaged over 13 hydrological stations, the difference between monthly anomalies is up to 100 cm (Fig. 2a). With respect to annual mean, WL anomaly in June reaches up to 61 cm, while WL anomaly in January drops to −43 cm. Hereafter, we define JJA (June–August) as the flood season for the PRD, and JFM (January–March) as the drought season.

The amplitude and phase of WL seasonal cycle substantially vary with individual sites (Figs. 2b–n). The largest amplitudes exceed 100–150 cm at upstream stations, e.g., Makou, Nanhua, Sanshui, and Zidong (Figs. 2b–h). At coastal stations close to the river mouths (Figs. 2i–n), e.g., Wanqinshaxi, Sanshankou, Nansha, and Hengmen, the amplitudes of WL seasonal cycle decrease to 15–20 cm. Moving toward the downstream stations (coastward), the peak of WL seasonal cycle gradually changes from June to October. These coastal stations (Figs. 2i–n) show bimodal seasonality in monthly WL with the October peak tending to overtake the June peak. This indicates two distinct factors forcing the seasonality of WL.

2) ATMOSPHERIC AND OCEANIC FORCING

With rainfall and SL being approximated as the atmospheric and oceanic forcing sources, here we investigate their influences on seasonality of PRD WL. Monthly precipitation anomaly over the Pearl River catchment (Fig. 3a) reaches its highest values of 150 mm month^{-1} in June, related to the East Asia Summer monsoon, and its lowest is −88 mm month^{-1} in January when the northeasterly winds in the low troposphere carry cold and dry air (e.g., Chang et al. 2005; Wang and Chen 2012). The seasonal cycle of precipitation matches well the WL seasonal cycle at the inland hydrological stations (Figs. 2c–g). The effect of regional precipitation can also be expressed by river discharge combined at Makou and Sanshui (Fig. 3b), which dominates waters flowing to the western and northern distributaries of PRD (Luo et al. 2007; Zhang et al. 2015). As expected, the monthly river discharge is firmly proportional to monthly WL anomalies at inland stations (Figs. 2c–g). The slight mismatch between the monthly rainfall and river
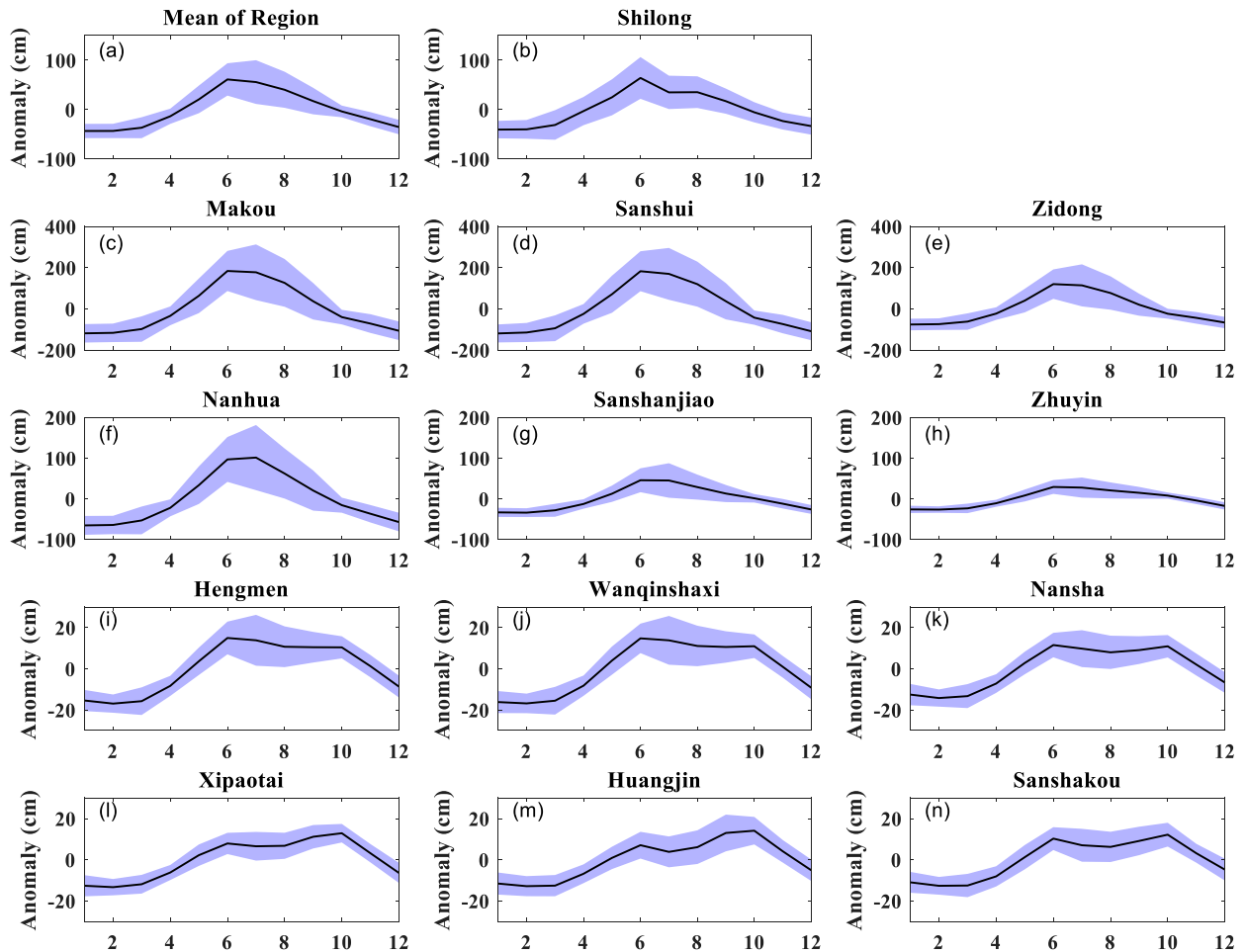
FIG. 2. WL monthly anomalies (a) averaged over the PRD, and (b)–(n) at individual stations (station names written as titles of individual panels). The solid line represents the mean of monthly anomalies (cm), and the shaded area is for the interannual spread (standard deviation) of monthly anomalies (cm), from 1961 to 2012.

discharge (Figs. 3a,b) may be due to the time lag between rainfall occurrence and the river discharge response.

Monthly SL anomaly at Hong Kong, an indicator of the oceanic forcing for PRD WL, is shown in Fig. 3c. The SL seasonal cycle has an amplitude of ~15 cm, peaking in October. At Hong Kong, the SL seasonal cycle is largely asymmetric in shape, i.e., with long-lasting negative anomalies and short-lasting

positive anomalies. The large positive anomaly in October is thought to be responsible for the second peak of monthly WL at the coastal stations (Figs. 2i–n). In the northern SCS, SL seasonality is mostly due to the sea surface current forced by the longshore wind, with the inverted barometer effect and seawater thermal expansion standing as the secondary forcing terms (Feng, et al. 2015).
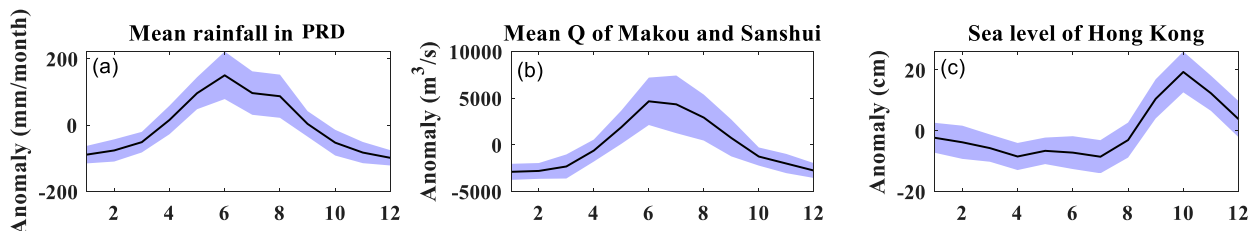

FIG. 3. Monthly anomalies calculated for 1961–2012 of (a) Pearl River catchment average rainfall (mm month^{-1}), (b) river discharge anomaly combined at Makou and Sanshui (m^3 s^{-1}), and (c) sea level at Hong Kong (cm). Solid line represents the mean of monthly anomalies, and shaded area is for the interannual spread (standard deviation) of monthly anomalies, from 1961 to 2012.
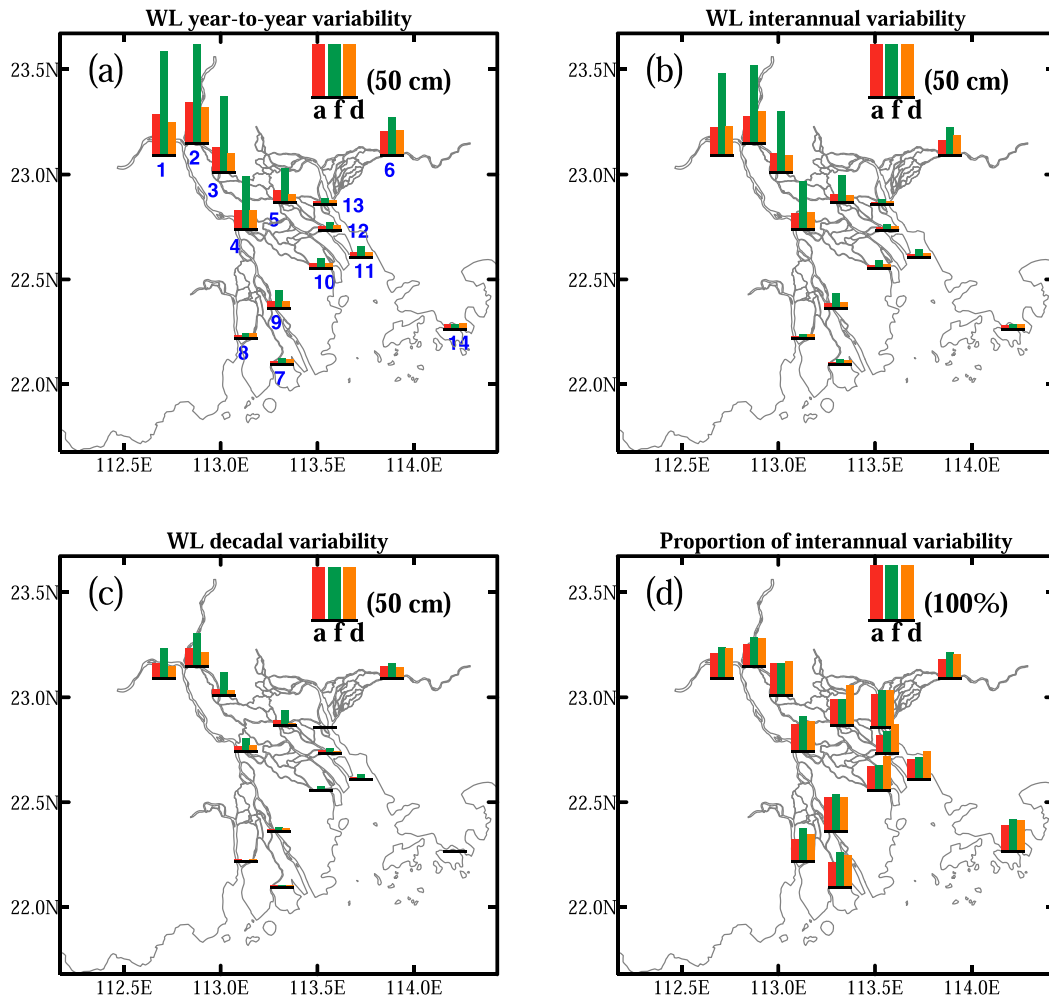
FIG. 4. (a) Standard deviation of WL long-term (detrended) variability (cm) for annual (red bar "a"), flood season (green bar "f") and drought season (orange bar "d") means, during 1961–2012. (b) As in (a), but for interannual (2–7 years; cm) time scales; (c) as in (a), but for decadal (>11 years; cm) time scales. (d) Proportion of WL interannual variations over the total variations [(b)/(a); %]. Values for SL at Hong Kong are also shown as the low right bars in each panel. In (a), the stations are numbered coastward from 1 to 14: 1) Makou, 2) Sanshui, 3) Zidong, 4) Nanhua, 5) Sanshanjiao, 6) Shilong, 7) Huangjin, 8) Xipaotai, 9) Zhuyin, 10) Hengmen, 11) Wanqinshaxi, 12) Nansha, 13) Sanshakou, and 14) Hong Kong.

The seasonality of WL at PRD coastal stations (Figs. 2i–n) is caused by the compound effects of regional SL and rainfall (Figs. 3b,c). In JJA, the southwesterly winds from the Indian ocean bring humid air and heave rainfall to southern China (e.g., Chang et al. 2005; Wang and Chen 2012; Feng et al. 2015), causing positive WL anomalies in the PRD. On the other hand, the southwesterly winds can also generate coastal Ekman pumping, making negative SL anomalies on the northwestern coasts of SCS. Conversely, in October–December (OND), the northeasterly winds cause positive SL anomalies on the SCS coasts, and usually bring little rainfall to the region. Thus, the seasonality of atmospheric and oceanic forcing, which has opposite effects on PRD WL, is not mutually independent. At the six coastal stations (Figs. 2i–n), the first peak of monthly WL anomaly is due to the predominance of

the atmospheric forcing over oceanic forcing, while the second peak is mostly related to the predominance of the oceanic forcing over atmospheric forcing. At the seven inland stations (Figs. 2b–h), SL has no detectable effect on WL seasonal variations.

Interannual spread (standard deviation) of monthly PRD WL anomaly is calculated (Fig. 2), to indicate the stationarity of the monthly anomalies over the 52 years after eliminating the effects of long-term variations and trend. Similar to WL means, the spread is usually larger in flood season and smaller in drought season, corresponding to the spreads of regional precipitation and river discharge (Figs. 3a–b). The largest average spread reaches up to 44 cm in July, and the spread dramatically decreases toward coasts (Fig. 2). At the coastal stations, the seasonality of WL spread tends to indistinctive
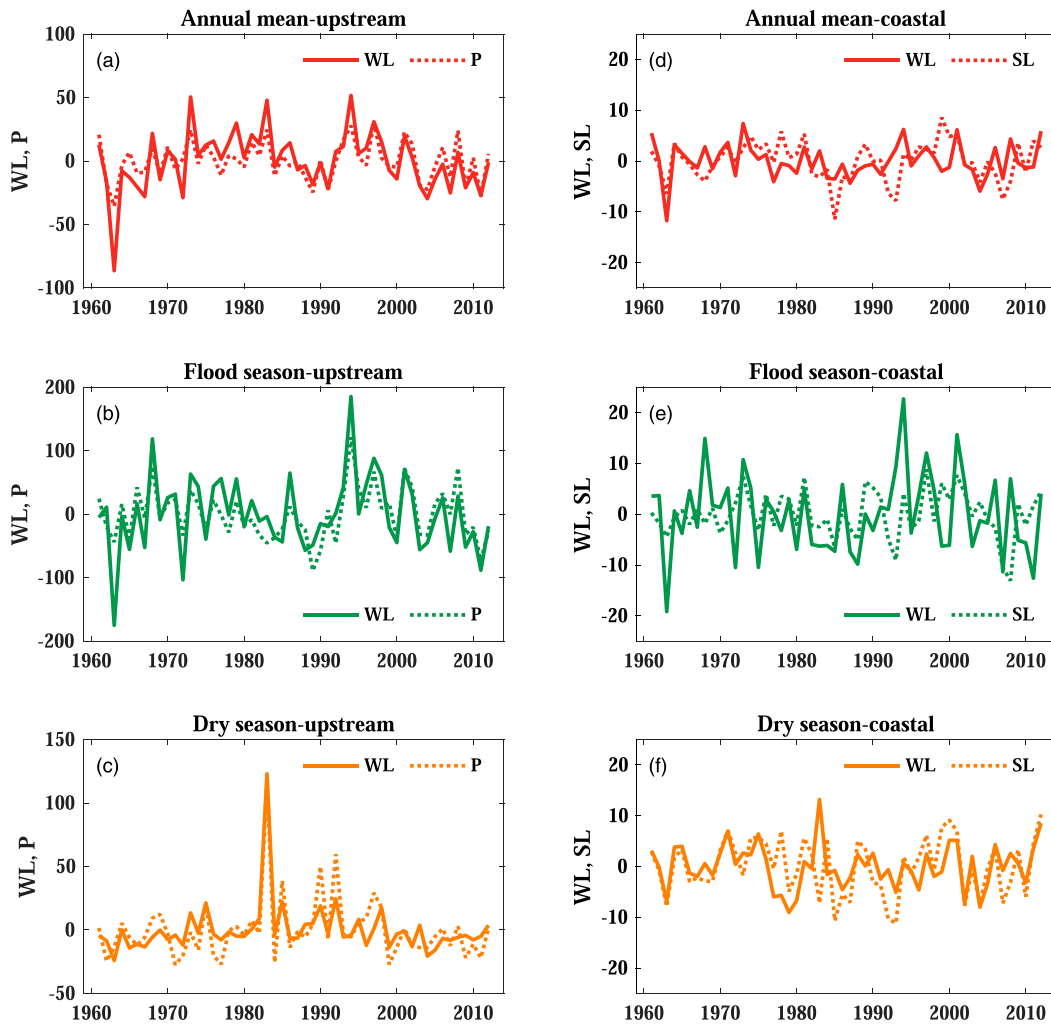
FIG. 5. Detrended time series of WL anomalies (solid lines; cm) averaged over upstream stations (station numbers 1–6 shown in Fig. 1a), and rainfall averaged over Pearl River catchment (dashed lines; mm month^{-1}), for (a) annual, (b) flood season, and (c) drought season means, over 1961–2012. (d)–(f) Detrended time series of WL anomalies (solid lines; cm) averaged over coastal stations (station numbers 7–13 shown in Fig. 1a), and SL anomalies at Hong Kong (dashed lines; cm), for (d) annual, (e) flood season, and (f) drought season means.

(Figs. 2i–n), related to the nearly constant spread in monthly SL anomalies (Fig. 3c).

b. Long-term variability in water level

1) VARIATIONS

In this subsection, we investigate the long-term variability in PRD WL. PRD WL exhibits apparent year-to-year (detrended) variability. The largest magnitude of WL year-to-year variability is at Makou, Sanshui, and Shilong (Fig. 4a), where the annual WL varies about 39, 39, and 24 cm, respectively, between different years. This indicates the overall large variations in the atmospheric forcing (this will be discussed in detail in next subsection). Conversely, coastal stations have small magnitude of WL variability (<10 cm), indicating the relatively less variations in oceanic forcing. The WL long-term variations are noticeably larger in flood season than in drought season. For example, at Makou and Sanshui, flood season WL varies by 98 and 94 cm between different years on average, which are 3 times the magnitude of variations in drought season.

We further decompose the long-term variability of WL into components on interannual (2–7 years; Fig. 4b) and decadal (>11 years; Fig. 4c) time scales. Annual and seasonal means of WL at each station are smoothed with a 7-yr low-pass filter during the observation period, and the difference between the original and smoothed variability is estimated as the interannual (2–7 years) variability. Similarly, an 11-yr low-pass filter is applied in the original time series, to retain the decadal (>11 years) variability. At PRD upstream stations, interannual variability of WL has a magnitude of 15–25, 45–80, and 15–30 cm for annual, flood season, and drought season means, respectively, which are much larger than the amplitudes at coastal stations, which are mostly <10 cm. WL decadal variability shows the

same spatial pattern among individual stations, but with a smaller amplitude. Figure 4d shows the percentage of standard deviation of interannual variability over that of the total variability (Figs. 4a,b). There are no clear spatial variations in the relative contributions of WL interannual (Fig. 4d) and decadal (not shown) variability. In general, interannual variations account for about 46%, 55%, and 57% of the total WL variations for annual, flood season, and drought season means, respectively.

2) ATMOSPHERIC AND OCEANIC FORCING

In this subsection, we evaluate the effects of atmospheric and oceanic forcing on long-term variability of WL. As mentioned before, our underlying assumption is that the two forcing sources can be represented by the Pearl River catchment rainfall and SL at Hong Kong. The long-term detrended correlations between the river catchment rainfall and Hong Kong SL are $r = 0.06$ and 0.02 (not significant at the 0.05 level) for annual and flood season means, respectively, suggesting the independence of SL from regional rainfall. For drought season, the two sources are correlated with $r = -0.31$ (significant at the 0.05 level), which could be related to the opposite effects of the large-scale climate variability (this will be discussed in detail in section 3c).

The long-term variability in WL average aggregated at six upstream stations (Makou, Sanshui, Zidong, Nanhua, Sanshanjiao, and Shilong) is well explained by rainfall in the river catchment (Figs. 5a–c). Significant correlations between overall WL and catchment rainfall for annual ($r = 0.81$), flood season ($r = 0.78$) and dry season ($r = 0.85$) are found, confirming rainfall is the key forcing factor in the long-term variability of upstream WL. We further find that for flood season the variability of upstream WL is mostly related to the rainfall in the central part of river catchment ($r > 0.80$; Fig. 6a), while for drought season it is mostly associated with the local rainfall (i.e., eastern part of the catchment; $r > 0.80$; Fig. 6b). This difference might be related to the different southern China rainfall regimes in summer and winter. When partitioning the regional average WL to components on different time scales, we found that rainfall in the central part of river catchment has a stronger influence on the interannual components than on the decadal components (Fig. S1 in the online supplemental material). This might be related to the larger spatial variations of rainfall on decadal time scales than on interannual time scales.

To further understand the impacts of atmospheric forcing on the spatial distributions of WL long-term variability, we calculate the spatial autocorrelation of WL variability in the PRD. Correlations of WL interannual (2–7 years) variability between the most upstream station (Sanshui) and other 12 stations are shown in Fig. 7a. For annual mean, the correlations are statistically significant at 0.05 level at all 12 stations, with $r = 0.55$–0.95. Except at three coastal stations, >50% of WL interannual variance can be explained by Sanshui WL. The correlations are stronger in flood season than in drought season, and they gradually decrease toward coasts. These suggest that on interannual time scales there is one dominant forcing source for PRD WLs from upstream to coastal stations. The dominance of atmospheric forcing is further confirmed with
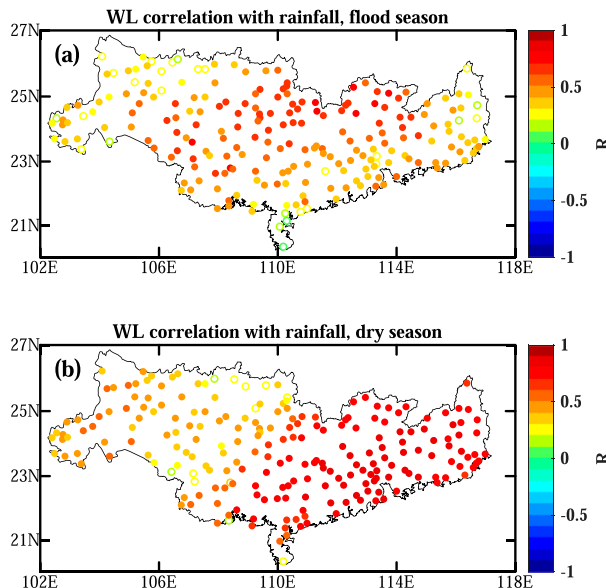

FIG. 6. Year-to-year (detrended) correlation coefficients between PRD average WL and rainfall at rain gauge stations in the Pearl River catchment, for (a) flood season and (b) drought season over 1961–2012. The solid circles indicate the correlations that that are significant at 0.05 level.

the robust relationships between WL at individual stations and the Pearl River catchment rainfall (Fig. 7b).

For decadal variability, annual WL at Sanshui is positively correlated with that at only 6 stations (mostly in upstream) (Fig. 7c). Negative decadal correlations with Sanshui WL are seen at coastal stations for drought season. The decadal relationships between WL and regional rainfall are largely consistent with the WL decadal autocorrelations (Figs. 7c,d). This suggests that on decadal time scales, PRD WL in flood season is mostly forced by the regional rainfall, but in drought season at coastal stations they are driven by multiple forcing factors. Same conclusions are drawn when using other upstream stations (e.g., Makou, Zidong, and Nanhua) in calculating the spatial autocorrelations.

SL has no significant effects on the long-term variability of regional aggregation of WL at upstream stations, while SL significantly modulates regional aggregate of WL at seven coastal stations ($r > 0.3$, significant at 0.05 level) (Fig. 5). At individual stations, interannual correlations between SL and PRD WL are shown in Fig. 7e. Significant correlations only appear at coastal locations ($r = 0.30$–0.59), with lower r values in flood season and higher r values in drought season. In flood season, SL is significantly correlated with WL at 5 stations (Wanqishaxi, Sanshakou, Nansha, Xipaotai, and Huangjing), while in dry season there is one additional station (Hengmen) where SL–WL correlation is significant ($r > 0.4$). Figure 7f presents the decadal SL–WL correlations. Clearly, compared to interannual correlations, SL has much stronger decadal correlations with PRD WL, especially for flood season. However, this does not necessarily mean a strong causal effect of oceanic forcing on decadal time scales. Instead, this is due in part to the same signs
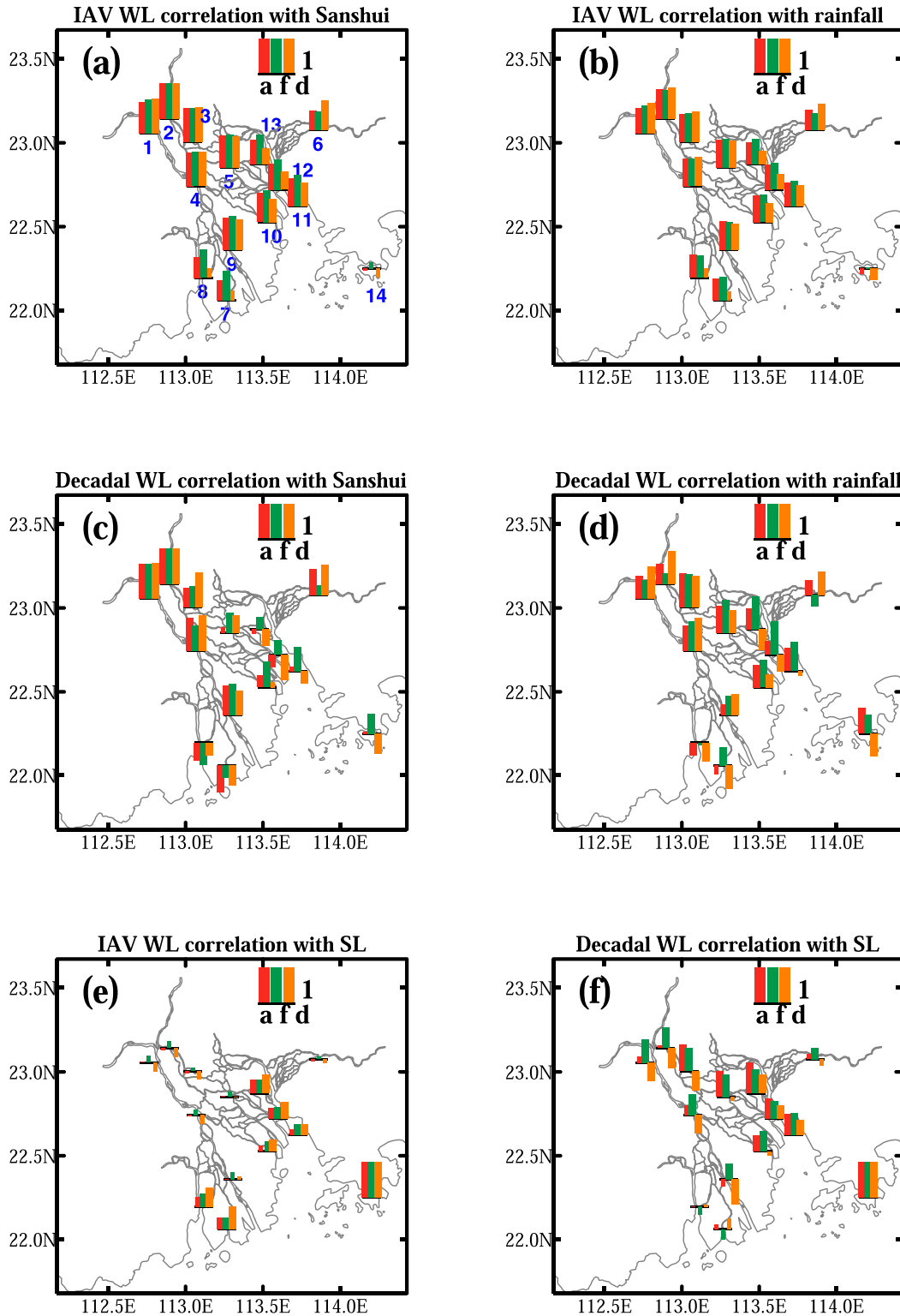
FIG. 7. As in Fig. 5, but for (a) interannual (2–7 years) correlation coefficients between WL at Sanshui and that at other stations for 1961–2012; (b) interannual (2–7 years) correlations between PRD rainfall and WL at all stations for 1961–2012. (c),(d) As in (a) and (b), but for decadal (>11 years) correlation coefficients. (e),(f) As in (c) and (d) but for correlations between SL at Hong Kong and WL at all stations. The thick bars indicate the correlations that are significant at 0.05 level. In (a), the stations are numbered coastward from 1 to 14: 1) Makou, 2) Sanshui, 3) Zidong, 4) Nanhua, 5) Sanshanjiao, 6) Shilong, 7) Huangjin, 8) Xipaotai, 9) Zhuyin, 10) Hengmen, 11) Wanqinshaxi, 12) Nansha, 13) Sanshakou, and 14) Hong Kong.

of teleconnections from PDO to rainfall and SL in flood season (see section 3c). Similarly, related to the opposite signs of teleconnections from PDO to rainfall and SL in drought season, in the most upstream and western distributary stations, WL decadal variations are negatively correlated with SL.

It is worth noting that our above diagnostics for the spatial coherence of WL variability in PRD (Fig. 7) could be interfered by the inhomogeneity of large-scale morphological changes. The differences of WL spatial autocorrelations and WL–rainfall correlations (Fig. 7a versus Fig. 7b, Fig. 7c versus Fig. 7d) imply other factors that may influence the WL variations in the PRD. This is especially true for the decadal variations. The cut depth of riverbed in the PRD is inhomogeneous with time and channels (e.g., Luo et al. 2007; Z. Wu et al. 2016; Tang et al. 2016). In the 1990s heavier river sand excavation happened in eastern river tributaries, while in the 2000s heavier riverbed cutdown occurred in the western tributaries. These inconsistent river morphological changes across space and time may have an unignorable impact on the coherence of WL variability across the PRD. Quantifying the effect of morphological changes is not the scope of this paper.

c. Effect of climate variability

To further understand the PRD WL long-term variability, we examine the teleconnections from the large-scale modes of climate variability. Similar to the decomposing analysis in WL, the 7-yr high-pass and 11-yr low-pass filters are applied to ENSO and PDO indices, to obtain their interannual (2–7 years) and decadal (>11 years) components (Figs. 8a,b). Figure 9a shows the interannual correlations between WL at individual stations and ENSO. During 1961–2012, the correlations between ENSO and flood season WL are not significant (at 0.05 level) at all hydrological stations. The lack of WL–ENSO relationships for flood season is associated with the weak teleconnections from ENSO to southern China rainfall (Fig. 10a). In flood season (JJA), the Pearl River catchment rainfall tends to have negative (positive) anomalies in El Niño (in La Niña) years. However, this relationship is not robust, which is consistent with previous studies (e.g., Mason and Goddard 2001; Chen et al. 2013; Ouyang et al. 2014; Wang et al. 2019, 2020). For the drought season (JFM), significant WL–ENSO correlations exist only at four upstream stations. This is related to the positive ENSO–rainfall teleconnections ($r = 0.3–0.5$) in the eastern part of the river basin. Evidently, WL and precipitation in the drought season of 1983 are outliers for the whole period (Figs. 5c, 8c). These values were thought to affect the diagnosed teleconnections from climate variability to WL and rainfall. However, we found that removal of these outliers does not change our above conclusions.

It is interesting to highlight the interdecadal changes in the WL–ENSO relationships. Studies suggested that the relationships between southern China rainfall and ENSO could vary with time, especially for winter and spring rainfalls, associated with different epochs of the interdecadal climate variability, such as PDO (e.g., Wang et al. 2009; Chen et al. 2014; Feng et al. 2014; Wu and Mao 2016). This could be hypothesized by the possible dependence of PDO on ENSO (Newman et al. 2016). We divide our WL records (1961–2012) into two periods,
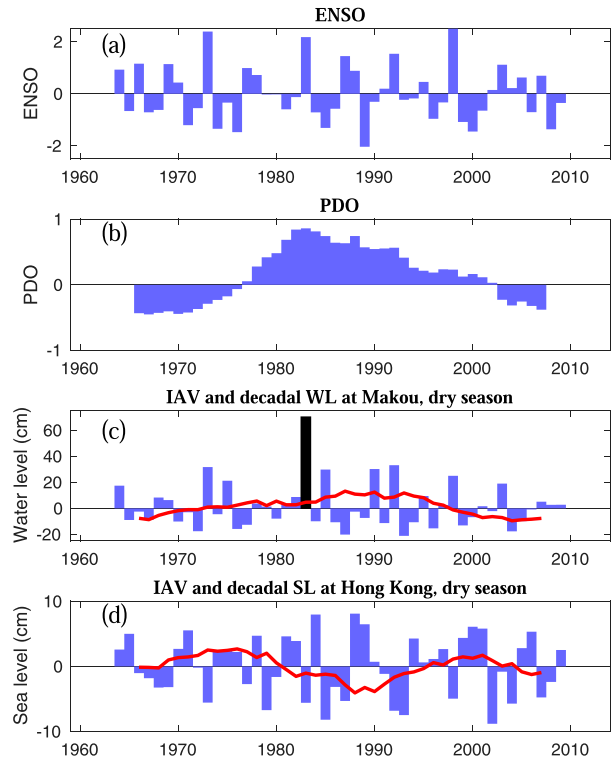

FIG. 8. Time series of (a) interannual (2–7 years) ENSO index and (b) decadal (>11 years) PDO index. (c) Time series of WL interannual (2–7 years; blue bar) and decadal (>11 years; red line) anomalies in drought season at Makou, excluding the 1983 outlier (black bar). (d) Time series of SL interannual (2–7 years; blue bar) and decadal (>11 years; red line) anomalies in drought season at Hong Kong,

conditional on PDO (Fig. 8b): 1961–84, the cold-to-warm PDO phase, and 1985–2012, the warm-to-cold PDO phase. Figures 9b and 9c show the interannual correlations between ENSO and WL specified for these two epochs, respectively. During 1961–84, there is a commonly positive WL–ENSO relationship, including at those coastal stations ($r = 0.2–0.4$, not statistically significant), with stronger correlations at upstream stations ($r > 0.4$, statistically significant). During 1985–2012, the WL–ENSO relationship becomes much weaker in upstream and turns to negative on the coasts.

In El Niño (La Niña) years, SL at Hong Kong tends to have negative (positive) anomalies (Figs. 8d, 9a). This SL–ENSO relationship is more pronounced in drought season than in flood season. This negative relationship is not observed at the coastal hydrological stations during 1961–2012 (Fig. 9a), confirming the dominance of atmospheric forcing in WL interannual variability at those stations (Figs. 7a,b). After dividing the whole period into two epochs (i.e., 1961–84 and 1985–2012) (Figs. 9b,c), we find that in the second epoch, negative WL–ENSO correlations consistently appear at coastal stations, although they are not always significant at 0.05 level. This means that ENSO has a stronger effect on the oceanic forcing of PRD WL in 1985–2012 than in 1961–84. Thus, we
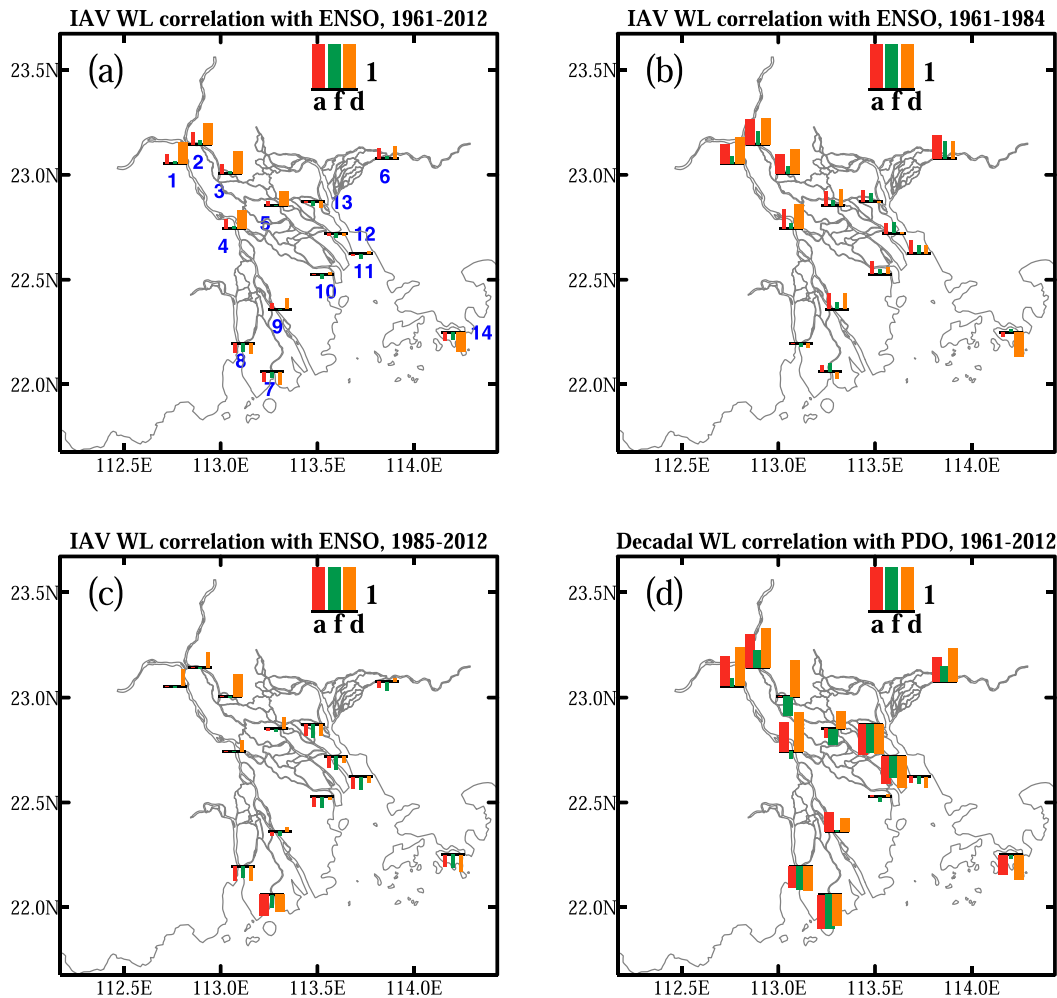
FIG. 9. As in Fig. 5, but for (a) interannual (2–7 years) correlation coefficients between WL and ENSO, over (a) 1961–2012, (b) 1961–84, and (c) 1985–2012. (d) Decadal (>11 years) correlation coefficients between WL and PDO, over 1961–2012. The thick bars indicate the correlations that are significant at 0.05 level. Values for SL at Hong Kong are also shown as the lower right bars in each panel. In (a), the stations are numbered coastward from 1 to 14: 1) Makou, 2) Sanshui, 3) Zidong, 4) Nanhua, 5) Sanshanjiao, 6) Shilong, 7) Huangjin, 8) Xipaotai, 9) Zhuyin, 10) Hengmen, 11) Wanqinshaxi, 12) Nansha, 13) Sanshakou, and 14) Hong Kong.

conclude that the ENSO–WL teleconnections are not stationary with time, and this is related to the interdecadal changes in the responses of atmospheric and oceanic forcing to ENSO.

The decadal variability of PRD WL is strongly modulated by PDO (Fig. 9d). Opposite correlations between WL and PDO are seen at inland and coastal stations. The correlations are $r = 0.4$–0.8 at upstream stations and $r = -0.4$ to -0.8 at most coastal stations. At upstream stations, the WL–PDO teleconnections are more pronounced in drought season than in flood season. This seasonal difference can be interpreted by the decadal variations of southern China rainfall (Figs. 10c,d). In the warm phases of PDO, the drought season rainfall in river catchment has significantly positive anomalies (even when the 1983 outliers are excluded, not shown), while the flood season rainfall has negative and less robust anomalies. Our results

about rainfall decadal variability are consistent with previous studies (Chan and Zhou 2005; D'Arrigo and Wilson 2006; Ouyang et al. 2014; Si and Ding 2016). At most of the coastal stations, the WL–PDO relationships are significantly negative (Fig. 9d). They are related to the decadal variability in SL, which is correlated with PDO, with $r > -0.45$ for annual and drought season means (Figs. 8d, 9d), consistent with previous studies (e.g., Feng and Tsimplis 2014; Cheng et al. 2016; Feng and Cheng 2019).

In short, the regional rainfall and SL have different responses to the climate variability (ENSO and PDO). This implies that climate variability can significantly alter the strengths of atmospheric and oceanic forcing of PRD WL. In the drought seasons of El Niño or warm PDO phases, due to increased southern China rainfall and negative SL anomalies, the effect of atmospheric forcing on PRD WL is enhanced. Conversely,
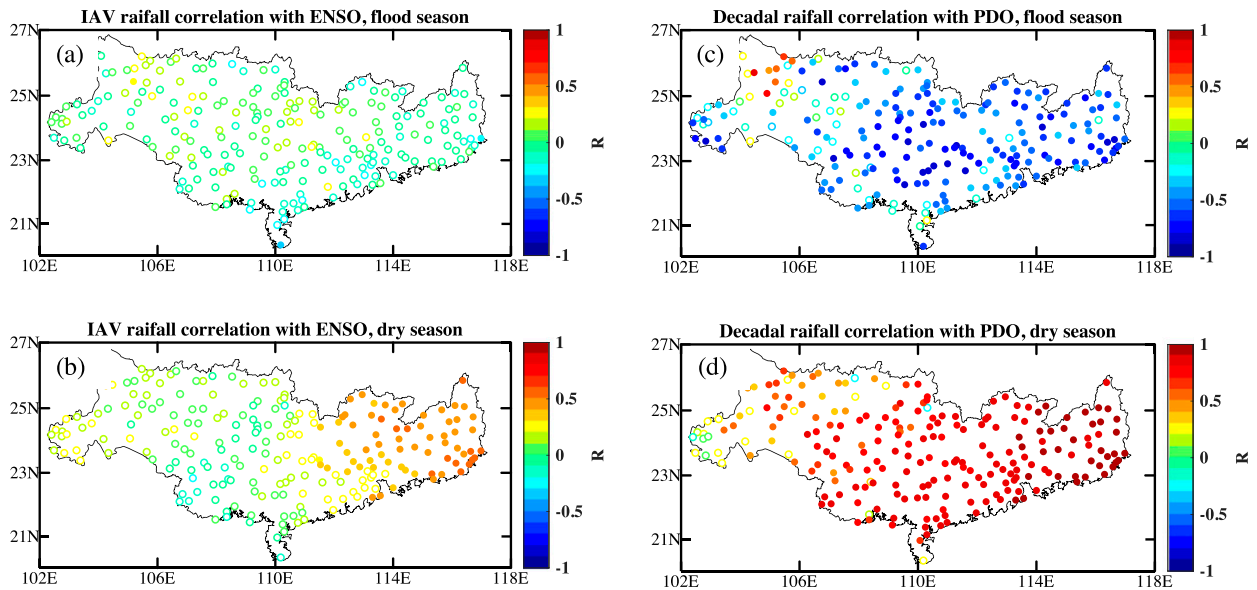
FIG. 10. Interannual correlation coefficients between ENSO and rainfall at rain gauge stations in the Pearl River catchment, for (a) flood season and (b) drought season, over 1961–2012. (c),(d) As in (a) and (b), but for decadal correlations with PDO. The solid circles indicate the correlations that are significant at 0.05 level.

the effect of oceanic forcing is enhanced in the years with La Niña or cold PDO phases. We recall the potential impacts of river morphological changes on the WL–PDO relationships. As mentioned before, the inhomogeneity of morphological changes between decades may play down the significance of the WL–PDO relationships.

d. Long-term trend of water level

Finally, we evaluate the long-term linear trends of PRD WL and associate them with the changes in the atmospheric and oceanic forcing. WL trend varies substantially among hydrological stations, with negative rates in upstream and positive rates toward coasts. WL average over the six upstream stations for annual, flood season and drought season means decreases significantly over 1961–2012, with rate of -1.52 ± 0.43, -2.61 ± 1.09, and $-0.39 \pm 0.38 \, \mathrm{cm \, yr^{-1}}$ (statistically significant at 0.05 level), respectively (Figs. 11a–c). For WL average over the seven coastal stations, it significantly increases by 0.14 ± 0.06 and $0.24 \pm 0.08 \, \mathrm{cm \, yr^{-1}}$ for annual and drought season means, respectively, but it has no trend for flood season means ($0.07 \pm 0.15 \, \mathrm{cm \, yr^{-1}}$) (Figs. 11d–f). More precisely, the western and eastern distributaries see the largest decreases from -2.40 to $-2.08 \, \mathrm{cm \, yr^{-1}}$, from -4.20 to $-2.81 \, \mathrm{cm \, yr^{-1}}$, and from -1.43 to $-0.47 \, \mathrm{cm \, yr^{-1}}$, for annual, flood season, and dry season means, respectively (Fig. 12a). At coastal stations, most of the positive trends are significant, in the range of 0.10– $0.43 \, \mathrm{cm \, yr^{-1}}$. In the transition zone (Zhuyin and Sanshanjiao), the trends are not statistically significant. We also reassessed the linear trends of WL at individual stations after removing the impacts of ENSO and PDO using multiple linear regression, to eliminate the effects of climate variability on trend detection (Fig. 12b). The removal of ENSO and PDO impacts reduces the magnitudes of negative trends of WL at upstream

stations, while it makes little change for the trends at coastal stations. The largest reduction of trend after removing the ENSO and PDO effects is 0.4–$0.5 \, \mathrm{cm \, yr^{-1}}$ at Makou and Sanshui. Therefore, the natural climate variability also plays a role in the linear trend detection.

Previous studies attributed the large decrease of WL upstream to intensive river-dredging and sand-mining activities in the PRD due to human activities (e.g., Luo et al. 2007; Zhang et al. 2008, 2011; Zhang et al. 2015; Z. Wu et al. 2016). The demand for sand significantly increased with the rapid economic development in the PRD since the 1980s. Unlike many other regions in the world (e.g., Pinter et al. 2004), there have been no official records for sand mining in PRD, because most of these activities were not officially permitted. This causes major difficulties in accurately assessing the river-dredging and sand-mining effects on the PRD WL trend. Another factor presumably responsible for the riverbed changes is the decline of the sediment load in water. Due to intensive constructions of dams and reservoirs in the upstream of the Pearl River since the 1950s, the sediment concentration rate in the PRD has decreased significantly (e.g., W. Zhang et al. 2012; Z. Wu et al. 2016; C. S. Wu et al. 2016; Wang et al. 2021). To maintain the normal sediment carrying capacity, more sediments are eroded from local riverbed and banks, which also dredge the river channel further deep and wide.

The amount of water flowing through the western distributaries of PRD is controlled by river discharge through Makou, while the waterflow in the northern distributaries is controlled by river discharge through Sanshui (Luo et al. 2007; Zhang et al. 2015). Annual river discharges at Makou and Sanshui are shown in Figs. 13a and 13b. Discharge at Makou is about 6 times that at Sanshui on average. During 1961–2012,
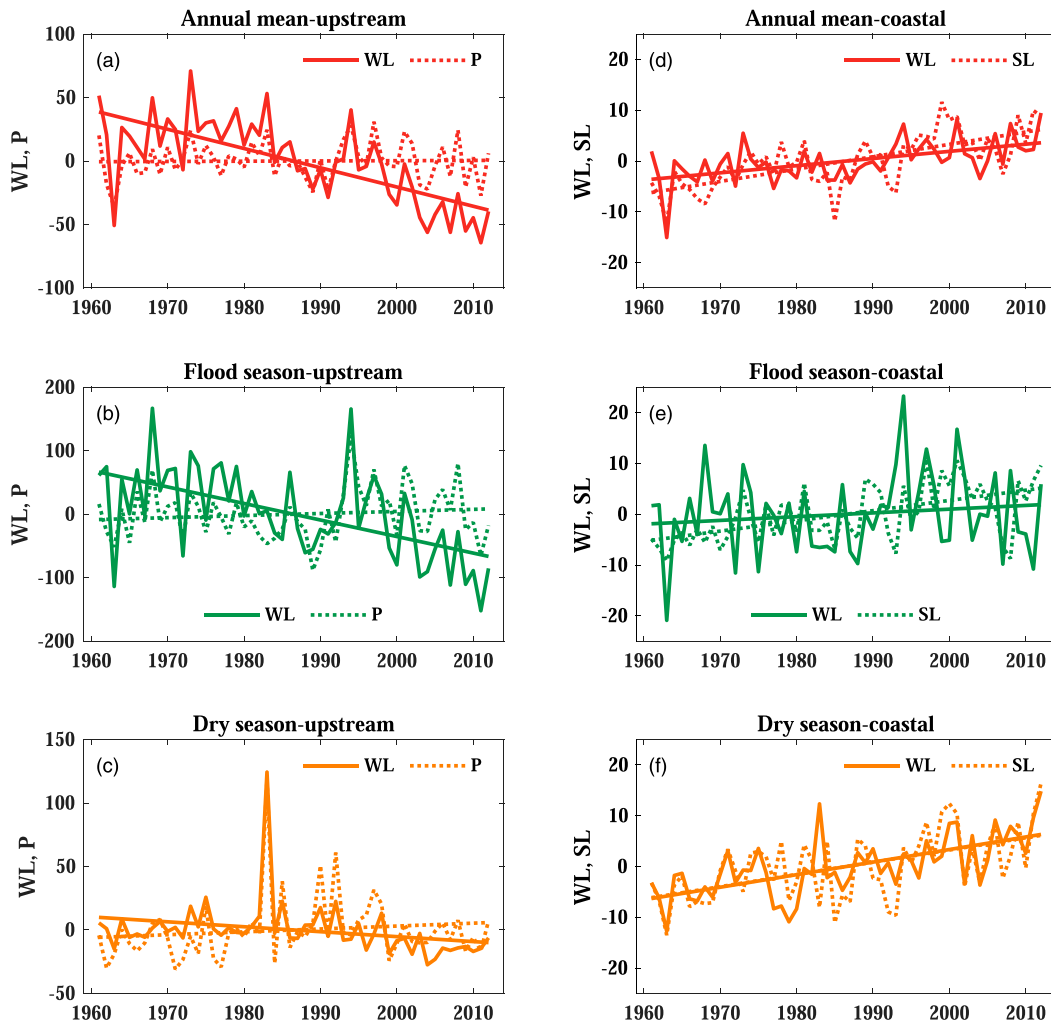
FIG. 11. Time series of WL anomalies (solid lines; cm) averaged over upstream stations (station numbers 1–6 shown in Fig. 1a), and rainfall averaged over Pearl River catchment (dashed lines; mm month^{-1}), for (a) annual, (b) flood season, and (c) drought season means, over 1961–2012. (d)–(f) Time series of WL anomalies (solid lines; cm) averaged over coastal stations (station numbers 7–13 shown in Fig. 1a), and SL anomalies at Hong Kong (dashed lines; cm), for (d) annual, (e) flood season, and (f) drought season means, over 1961–2012. Straight lines show the linear trends.

discharge at Makou has slightly decreased by $-27 \pm 24 \, m^3 \, s^{-1} \, yr^{-1}$. In contrast, discharge at Sanshui has increased by $16 \pm 8 \, m^3 \, s^{-1} \, yr^{-1}$. These changes are related to the change of streamflow ratio between Makou and Sanshui, probably due to the spatially unbalanced sand excavation of riverbed over the past decades (Luo et al. 2007; Zhang et al. 2015). This suggests that the large WL decrease in the western distributaries (Fig. 12a) is likely due to the compound effects of river discharge reduction and riverbed change. In the northern distributaries, river discharge increase could be partially responsible for the WL increase. After combining the two stations (Fig. 13c), the discharge trends become insignificant, with values of -7 ± 31, 12 ± 82, and $17 \pm 27 \, m^3 \, s^{-1} \, yr^{-1}$ for annual, flood season and dry season means, respectively. This corresponds to the insignificant changes in the Pearl River catchment rainfall (Figs. 11a–c). Thus, we conclude

that the atmospheric forcing is not responsible for the overall decrease of PRD WL over 1961–2012, although redistribution of river discharge among distributaries may affect the spatial variations of the trend.

It is worth noticing a changepoint of river discharge around 1994. There is a significant decrease in river discharge during 1994–2012, at rate of -142 ± 99 and $-50 \pm 44 \, m^3 \, s^{-1} \, yr^{-1}$ at Makou and Sanshui, respectively, contrasting an unclear change there before (Figs. 13a,b). After combining the two stations, there is still a large downward trend in river discharge in flood season (Fig. 13c). A downward trend is also observed in the catchment precipitation in flood season over this period (Fig. 11b). The changes in southern China precipitation and river discharge during 1994–2012 could be associated with a regime shift of large-scale environments, such as the transitioning of PDO from positive to negative phases (Fig. 8b).
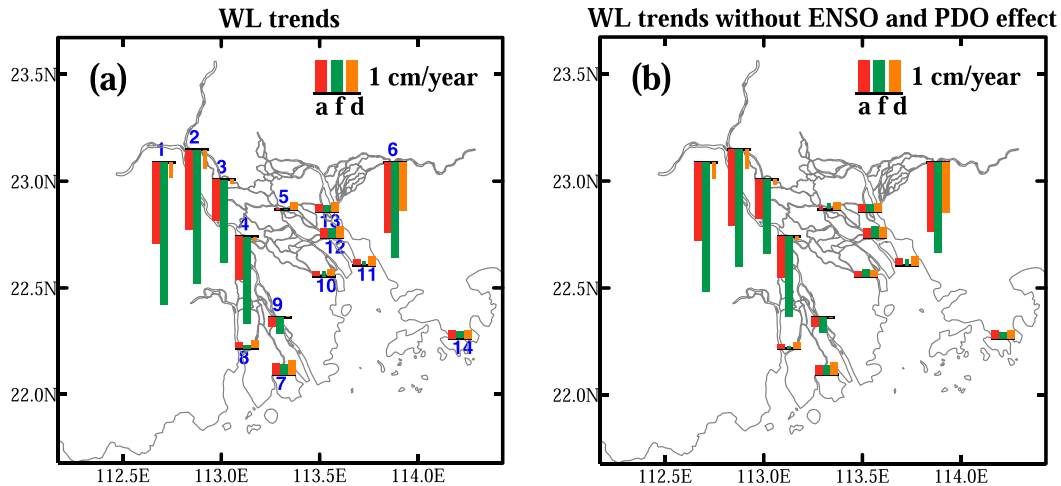
FIG. 12. (a) WL linear trends for annual (red bar ''a''), flood season (green bar ''f''), and drought season (orange bar ''d'') means, during 1961–2012. (b) As in (a), but for WL linear trends after the effects of ENSO and PDO are removed using a multiple linear regression. The thick bars indicate the trends that are significant at 0.05 level. Values for SL at Hong Kong are also shown as the lower-right bars in each panel. In (a), the stations are numbered coastward from 1 to 14: 1) Makou, 2) Sanshui, 3) Zidong, 4) Nanhua, 5) Sanshanjiao, 6) Shilong, 7) Huangjin, 8) Xipaotai, 9) Zhuyin, 10) Hengmen, 11) Wanqinshaxi, 12) Nansha, 13) Sanshakou, and 14) Hong Kong.

Human activities may also play a role in the fast reduction of river discharge over this period, such as water consumption for agriculture and industry. We highlight that upstream WL does not change monotonically over the whole period, with a faster decrease in 1994–2012 than in the prior period (Figs. 11a–c), suggesting the combined impacts of reduced atmospheric forcing and human activities.

SL at Hong Kong shows steady and significant increase (Figs. 11d–f), with 0.24 ± 0.07, 0.20 ± 0.09, and 0.24 ± 0.10 cm yr^{-1} for annual, flood season, and dry season means, respectively. These trends are close to those WL trends at coastal stations. At these coastal stations, removing SL anomalies from WL anomalies diminishes the positive trends or makes the trends slightly negative (not shown). This suggests the dominance of SL in the WL trends at coastal stations. Noticeably, WL trends at upstream stations for drought season are small and insignificant (Fig. 12). This might be due to two reasons. First, in drought season, as seawater intrudes further upstream, the sea level rise reduces or counteracts the decrease trend of WL at these upstream stations associated with morphological changes of river. Second, a large number of dams have been built along PRD river networks, to secure the minimum WL for water resource security and shipping safety (e.g., Liu et al. 2017). The maintenance of minimum WL could also be responsible for these small negative trends.

4. Conclusion and discussions

Evaluating and attributing the variability and changes in PRD WL are important for managing water resources and reducing flood/drought risks. There are multiple factors affecting the PRD WL. However, most of previous studies focused on the anthropogenic influence on the long-term changes

of PRD WL. In this paper, we investigated the causal effects of the atmospheric and oceanic forcing on the PRD WL on time scales from seasonal to decadal, using more than 50 years of in situ observations. We approximated the Pearl River catchment rainfall and sea level at the northern coasts of SCS as the indicators of the atmospheric and oceanic forcing for PRD WL, respectively.

WL in the PRD presents significant seasonality, with the amplitudes > 100 cm at the upstream stations and <20 cm at the coastal stations. At the upstream stations, WL peak occurs in June, associated with the heavy rainfall due to the East Asia summer monsoon, and WL trough occurs in January. At the coastal stations, WL has a second peak in October, which tends to overtake the June peak, making the June peak less outstanding. The dual peak in seasonal WL at coastal stations can be explained by the dependence of atmospheric and oceanic forcing. In flood season (June–August), the East Asia summer monsoon brings heavy rainfall to southern China, accompanied with strong southwesterly winds. These southwesterly winds in turn can drive a coastal Ekman pumping, causing negative SL anomalies on the southern China coasts. This oceanic response likely reduces the positive WL anomalies at the coastal stations due to the atmospheric forcing. In October–December, conversely, when the northeasterly winds bring little rainfall to this region, the oceanic forcing is dominant, and this causes anomalous SL elevations on the coasts. Thus, the two peaks in seasonal WL at coastal stations are associated with the combined effects of atmospheric and oceanic forcing. Further numerical tests will help to quantitatively evaluate the seasonal WL anomalies forced by each natural forcing.

On interannual to decadal time scales, the largest magnitudes (25–40 cm) of WL variability were found at upstream stations, with the smallest (<10 cm) at coastal stations.
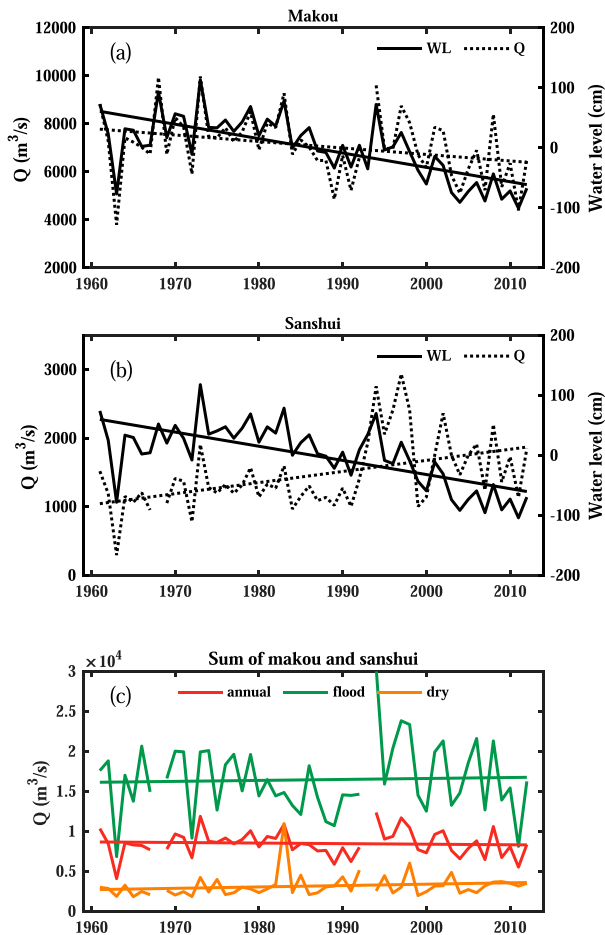
FIG. 13. Time series of annual-mean river discharge (dashed line; Q; m^3 s^{-1}; left y axis) and WL anomalies (solid line; cm; right y axis) at (a) Makou and (b) Sanshui. Note that WL anomalies are calculated in reference to the 1961–2012 period. (c) Time series of river discharge (Q; m^3 s^{-1}) for annual, flood season and drought season means, after combining values at Makou and Sanshui. Straight lines show the linear trends for the periods of 1961–2012.

On interannual (2–7 years) time scales, southern China rainfall is the dominant force for the overall variability of PRD WL, while the regional SL is only responsible for WL variability in drought season at limited stations. For the decadal (>11 years) variability of PRD WL, both southern China rainfall and regional SL play an important role. We further found that ENSO and PDO can significantly alter the competing effects of atmospheric and oceanic forcing, and this is particularly the case for the drought season. The WL–ENSO teleconnections are not stationary with time, which are stronger during 1961–84 and weaker during 1985–2012. In the years of El Niño or warm PDO phases, due to increased southern China rainfall and negative SL anomalies, the strength of atmospheric (oceanic) forcing is enhanced (weakened). This also implies that in the cold phases of ENSO and PDO, due to higher SL and less rainfall, seawater can go upriver further and impede river drainage for a longer time. This will increase the risk of saltwater intrusion and riverine flooding once oceanic extremes

(e.g., storm surge) occur. In the future, it is worth stratifying the coastal hazards in PRD by conditioning on the large-scale modes of climate variability.

Over the whole observational period, the overall WL in PRD decreased about 6 and 12 mm yr^{-1} for annual and flood season means. Spatially, upstream stations saw the largest decrease trends, whereas the coastal stations had the upward trends. The effect of atmospheric forcing explains little of the observed trends in WL. Mean SL is rising by >2 mm yr^{-1} in the northern part of SCS. This can explain most of WL increase at coastal stations and counteract partially WL reduction at the transition zone. Most of the observed decrease of WL at upstream stations was thought to relate to the enormous morphological changes due to intensive human activity.

In our analysis, it is difficult to further quantify how much the observed variations and changes in WL are caused by the atmospheric and oceanic forces individually. We will address this challenge in the future through sensitivity experiments, e.g., by running hydrodynamical models. We must be cautious of the exclusion of anthropogenic forcing in our analysis, which may potentially affect our results. Those factors include the inconsistent riverbed changes between periods and river channels due to sand mining and sediment flux changes, and river flow management by controlling dams for minimizing flood and drought risk. Differentiating the causal effects of natural and anthropogenic forcing on hydrological changes of river deltas would require sophisticated sensitivity experiments.

REFERENCES

Cao, Y., W. Zhang, Y. Zhu, X. Ji, Y. Xu, Y. Wu, and A. J. F. Hoitink, 2020: Impact of trends in river discharge and ocean tides on water level dynamics in the Pearl River Delta. *Coast. Eng.*, **157**, 103634, https://doi.org/10.1016/j.coastaleng.2020.103634.

Chan, J. C., and W. Zhou, 2005: PDO, ENSO and the early summer monsoon rainfall over south China. *Geophys. Res. Lett.*, **32**, L08810, https://doi.org/10.1029/2004GL022015.

Chang, C.-P., Z. Wang, J. McBride, and C. Liu, 2005: Annual cycle of Southeast Asia–Maritime Continent rainfall and the asymmetric monsoon transition. *J. Climate*, **18**, 287–301, https://doi.org/10.1175/JCLI-3257.1.

——, Y. Lei, C. H. Sui, X. Lin, and F. Ren, 2012: Tropical cyclone and extreme rainfall trends in East Asian summer monsoon since mid-20th century. *Geophys. Res. Lett.*, **39**, 18702, https://doi.org/10.1029/2012GL052945.

Chen, J., Z. Wen, R. Wu, Z. Chen, and P. Zhao, 2014: Interdecadal changes in the relationship between southern China winter-spring precipitation and ENSO. *Climate Dyn.*, **43**, 1327–1338, https://doi.org/10.1007/s00382-013-1947-x.

Chen, W., J. Feng, and R. Wu, 2013: Roles of ENSO and PDO in the link of the East Asian winter monsoon to the following summer monsoon. *J. Climate*, **26**, 622–635, https://doi.org/10.1175/JCLI-D-12-00021.1.

Chen, Y. D., Q. Zhang, T. Yang, C. Xu, X. Chen, and T. Jiang, 2007: Behaviors of extreme water level in the Pearl River Delta and possible impacts from human activities. *Hydrol. Earth Syst. Sci. Discuss.*, **4**, 4361–4387, https://doi.org/10.5194/hessd-4-4361-2007.

Cheng, X., S. P. Xie, Y. Du, J. Wang, X. Chen, and J. Wang, 2016: Interannual-to-decadal variability and trends of sea level in the South China Sea. *Climate Dyn.*, **46**, 3113–3126, https://doi.org/10.1007/s00382-015-2756-1.

D'Arrigo, R., and R. Wilson, 2006: On the Asian expression of the PDO. *Int. J. Climatol.*, **26**, 1607–1617, https://doi.org/10.1002/joc.1326.

Deng, S., T. Chen, N. Yang, L. Qu, M. Li, and D. Chen, 2018: Spatial and temporal distribution of rainfall and drought characteristics across the Pearl River basin. *Sci. Total Environ.*, **619–620**, 28–41, https://doi.org/10.1016/j.scitotenv.2017.10.339.

Duan, A., M. Wang, Y. Lei, and Y. Cui, 2013: Trends in summer rainfall over China associated with the Tibetan Plateau sensible heat source during 1980–2008. *J. Climate*, **26**, 261–275, https://doi.org/10.1175/JCLI-D-11-00669.1.

Feng, J., L. Wang, and W. Chen, 2014: How does the East Asian summer monsoon behave in the decaying phase of El Niño during different PDO phases? *J. Climate*, **27**, 2682–2698, https://doi.org/10.1175/JCLI-D-13-00015.1.

Feng, X., and M. N. Tsimplis, 2014: Sea level extremes at the coasts of China. *J. Geophys. Res. Oceans*, **119**, 1593–1608, https://doi.org/10.1002/2013JC009607.

——, and Y. Cheng, 2019: Observing sea levels in the China Seas from satellite altimetry. *Remote Sensing of the Asian Seas*, V. Barale and M. Gade, Eds., Springer, 321–338.

——, M. N. Tsimplis, M. Marcos, F. M. Calafat, J. Zheng, G. Jordà, and P. Cipollini, 2015: Spatial and temporal variations of the seasonal sea level cycle in the northwest Pacific. *J. Geophys. Res. Oceans*, **120**, 7091–7112, https://doi.org/10.1002/2015JC011154.

Liu, H. Z., X. Zhang, and W. W. Shao, 2017: Analysis on the law of water utilization structure in the progress of urbanization and industrialization and research on countermeasures of water supply security. *Renmin Zhujiang*, **38**, 10–14.

Luo, X. L., E. Y. Zeng, R. Y. Ji, and C. P. Wang, 2007: Effects of in-channel sand excavation on the hydrology of the Pearl River Delta, China. *J. Hydrol.*, **343**, 230–239, https://doi.org/10.1016/j.jhydrol.2007.06.019.

Mason, S. J., and L. Goddard, 2001: Probabilistic precipitation anomalies associated with ENSO. *Bull. Amer. Meteor. Soc.*, **82**, 619–638, https://doi.org/10.1175/1520-0477(2001)082<0619:PPAAWE>2.3.CO;2.

Newman, M., and Coauthors, 2016: The Pacific decadal oscillation, revisited. *J. Climate*, **29**, 4399–4427, https://doi.org/10.1175/JCLI-D-15-0508.1.

Ouyang, R., W. Liu, G. Fu, C. Liu, L. Hu, and H. Wang, 2014: Linkages between ENSO/PDO signals and precipitation, streamflow in China during the last 100 years. *Hydrol. Earth Syst. Sci.*, **18**, 3651–3661, https://doi.org/10.5194/hess-18-3651-2014.

Pinter, N., K. Miller, J. H. Wlosinski, and R. R. van der Ploeg, 2004: Recurrent shoaling and channel dredging, Middle and Upper Mississippi River, USA. *J. Hydrol.*, **290**, 275–296, https://doi.org/10.1016/j.jhydrol.2003.12.021.

Si, D., and Y. Ding, 2016: Oceanic forcings of the interdecadal variability in East Asian summer rainfall. *J. Climate*, **29**, 7633–7649, https://doi.org/10.1175/JCLI-D-15-0792.1.

Storto, A., A. Bonaduce, X. Feng, and C. Yang, 2019: Steric sea level changes from ocean reanalyses at global and regional scales. *Water*, **11**, 1987, https://doi.org/10.3390/w11101987.

Tang, Y., S. Xi, X. Chen, and Y. Lian, 2016: Quantification of multiple climate change and human activity impact factors on flood regimes in the Pearl River Delta of China. *Adv. Meteor.*, **2016**, 3928920, https://doi.org/10.1155/2016/3928920.

Wang, B., F. Huang, Z. Wu, J. Yang, X. Fu, and K. Kikuchi, 2009: Multi-scale climate variability of the South China Sea monsoon: A review. *Dyn. Atmos. Oceans*, **47**, 15–37, https://doi.org/10.1016/j.dynatmoce.2008.09.004.

——, X. Luo, and J. Liu, 2020: How robust is the Asian precipitation–ENSO relationship during the industrial warming period (1901–2017)? *J. Climate*, **33**, 2779–2792, https://doi.org/10.1175/JCLI-D-19-0630.1.

Wang, H., and H. Chen, 2012: Climate control for southeastern China moisture and precipitation: Indian or East Asian monsoon? *J. Geophys. Res.*, **117**, D12109, https://doi.org/10.1029/2012JD017734.

Wang, Q., W. Cai, W. Zhong, L. Zeng, L. Wu, and D. Wang, 2019: Response of southern China winter rainfall to El Niño diversity and its relevance to projected southern China rainfall change. *J. Climate*, **32**, 3343–3356, https://doi.org/10.1175/JCLI-D-18-0571.1.

Wang, Y. H., S. L. Cai, Y. D. Yang, Z. Y. Zhong, and F. Liu, 2021: Morphological consequences of upstream water and sediment changes and estuarine engineering activities in Pearl River Estuary channels over the last 50 years. *Sci. Total Environ.*, **765**, 144172, https://doi.org/10.1016/j.scitotenv.2020.144172.

Wu, C. S., S. Yang, S. Huang, and J. Mu, 2016: Delta changes in the Pearl River estuary and its response to human activities (1954–2008). *Quat. Int.*, **392**, 147–154, https://doi.org/10.1016/j.quaint.2015.04.009.

Wu, X., and J. Mao, 2016: Interdecadal modulation of ENSO-related spring rainfall over South China by the Pacific Decadal Oscillation. *Climate Dyn.*, **47**, 3203–3220, https://doi.org/10.1007/s00382-016-3021-y.

Wu, Z., and Coauthors, 2016: Impact of human activities on sub-aqueous topographic change in Lingding Bay of the Pearl River estuary, China, during 1955–2013. *Sci. Rep.*, **6**, 37742, https://doi.org/10.1038/srep37742.

Ye, J., W. Li, L. Li, and F. Zhang, 2013: ''North drying and south wetting'' summer precipitation trend over China and its potential linkage with aerosol loading. *Atmos. Res.*, **125–126**, 12–19, https://doi.org/10.1016/j.atmosres.2013.01.007.

Zhang, S., X. X. Lu, D. L. Higgitt, C. T. A. Chen, J. Han, and H. Sun, 2008: Recent changes of water discharge and sediment load in the Zhujiang (Pearl River) Basin, China. *Global Planet. Change*, **60**, 365–380, https://doi.org/10.1016/j.gloplacha.2007.04.003.

Zhang, Q., Y. D. Chen, T. Jiang, X. Chen, and Z. Liu, 2011: Human-induced regulations of river channels and implications for hydrological alterations in the Pearl River Delta, China. *Stochastic Environ. Res. Risk Assess.*, **25**, 1001–1011, https://doi.org/10.1007/s00477-011-0456-x.

——, V. P. Singh, J. Peng, Y. D. Chen, and J. Li, 2012: Spatial–temporal changes of precipitation structure across the Pearl River basin, China. *J. Hydrol.*, **440–441**, 113–122, https://doi.org/10.1016/j.jhydrol.2012.03.037.

Zhang, W., Y. Yan, J. Zheng, L. Li, X. Dong, and H. Cai, 2009: Temporal and spatial variability of annual extreme water level in the Pearl River Delta region, China. *Global Planet. Change*, **69**, 35–47, https://doi.org/10.1016/j.gloplacha.2009.07.003.

——, X. Wei, Z. Jinhai, Z. Yuliang, and Y. Zhang, 2012: Estimating suspended sediment loads in the Pearl River Delta region

using sediment rating curves. *Cont. Shelf Res.*, **38**, 35–46, https://doi.org/10.1016/j.csr.2012.02.017.

——, Y. Xu, A. J. F. Hoitink, M. G. Sassi, J. Zheng, X. Chen, and C. Zhang, 2015: Morphological change in the Pearl River Delta, China. *Mar. Geol.*, **363**, 202–219, https://doi.org/10.1016/j.margeo.2015.02.012.

Zhao, P., S. Yang, and R. Yu, 2010: Long-term changes in rainfall over eastern China and large-scale atmospheric circulation associated with recent global warming. *J. Climate*, **23**, 1544–1562, https://doi.org/10.1175/2009JCLI2660.1.

Zhao, Q., Q. Liu, L. Ma, S. Ding, S. Xu, C. Wu, and P. Liu, 2017: Spatiotemporal variations in rainfall erosivity during the period of 1960–2011 in Guangdong Province, southern China. *Theor. Appl. Climatol.*, **128**, 113–128, https://doi.org/10.1007/s00704-015-1694-5.